Aleksander Hejna, Józef Haponiuk, Łukasz Piszczyk, Marek Klein and Krzysztof Formela*

Performance properties of rigid polyurethane-polyisocyanurate/brewers' spent grain foamed composites as function of isocyanate index

DOI 10.1515/epoly-2017-0012
Received January 17, 2017; accepted May 8, 2017; previously published online June 23, 2017

Abstract: In the presented work, rigid polyurethane-polyisocyanurate (PUR-PIR) foams filled with brewers' spent grain (BSG) were prepared. The influence of the isocyanate index (II) on its performance was investigated. Foams obtained with higher isocyanate index required a higher amount of hydrofluorocarbon physical blowing agent to provide the same apparent density of material. An increase of isocyanate index resulted in a slight decrease of cell size, which was related to the increased crosslink density due to enhanced generation of allophanate and biuret groups. Deterioration of compressive strength, from 226 to 202 kPa was observed with the rise of the isocyanate index. Dynamic mechanical analysis and swelling tests confirmed the increase of crosslink density with the increasing isocyanate index. The glass transition temperature rose from 165.7°C to 193.2°C. Fourier transform infrared (FTIR) analysis indicated an increase of the isocyanurate rings' content in composites with a higher isocyanate index, causing noticeable enhancement of thermal stability. The onset of degradation was shifted from 196°C to 211°C.

Keywords: brewers' spent grain; environmentally-friendly composites; isocyanate index; rigid polyurethane-polyisocyanurate foams; thermal properties.

1 Introduction

Polyurethane (PUR) foams are very versatile materials, with multiple commercial applications. They are widely used in many branches of industry, therefore a lot of researchers' attention is paid to this group of materials. Nowadays, there are two main directions of research related to PUR foams: (i) enhancement of the recipe in order to obtain material with the best possible properties for specific applications and (ii) improvement of the ecological and economic aspects of production. The first trend can be observed in case of materials used in the electronic or automotive industries, where its performance can be important for human safety. In case of the second trend, there are different directions in the enhancement of the ecological aspect of PUR foams. Among them it is worth mentioning the use of bio-based polyols obtained from, e.g. rapeseed oil or crude glycerol (1, 2), incorporation of waste materials such as ground tire rubber (3–5) or ashes (6) or bio-based ones (7–9) such as as fillers in foamed polyurethane matrix.

Many different materials have been used as biofillers in PUR foams, such as cellulose, starch and more complex ones such as various lignocellulose fibers, wood flour, distillers' grains or other types of biomass (10–13). Generally, the most promising from the economic and technological points of view are materials, which are low-cost by-products from various industrial processes. A very good example of such material is brewers' spent grain (BSG), which is a high-volume by-product of the brewing industry. It amounts to ~85% of beer industry by-products (14). Currently, the amount of BSG generated only in Europe exceeds 2.5 million tonnes annually (15). Due to its high nutrient value and protein content, BSG is currently used mainly for animal nutrition, especially for cows, as it is increases milk production (16). Other investigated applications include human nutrition (17), energy production (18), cultivation of microorganisms (19) or incorporation into various biotechnological processes such as lactic acid or xylitol production (20).

Generally, the composition of BSG is very similar to other types of cellulosic fillers previously examined as modifiers enhancing the properties of PUR materials. Nevertheless, there is very little information in the literature regarding the application of BSG as a filler for polymer composites. However, the successful incorporation of this material into a foamed PUR matrix could

***Corresponding author: Dr. Krzysztof Formela,** Department of Polymer Technology, Chemical Faculty, Gdansk University of Technology, Gdansk, Poland, Tel.: +48 58 347 2234, Fax: +48 58 347 2134, e-mail: kformela.ktp@gmail.com; krzysztof.formela@pg.gda.pl
Aleksander Hejna, Józef Haponiuk and Łukasz Piszczyk: Department of Polymer Technology, Chemical Faculty, Gdansk University of Technology, Gdansk, Poland
Marek Klein: Renewable Energy Department, The Szewalski Institute of Fluid-Flow Machinery, Polish Academy of Sciences, Gdansk, Poland

increase the value of BSG, which will be also economically beneficial for the brewing industry. Therefore, in presented paper we aimed to prepare the biocomposites based on rigid polyurethane-polyisocyanurate (PUR-PIR) foams filled with BSG. Potential advantages of such BSG application include reduction of the price of composites, through incorporation of low-cost by-products into polymer matrixes and enhancement of profitability of beer production through the valorization of BSG. Moreover, during manufacturing of foams, crude glycerol-based polyol was applied, which reduced the amount of petrochemical polyols used. Therefore, two types of waste materials, resulting from the processing of renewable raw materials, were used for the preparation of analyzed biocomposites. The influence of a very important processing parameter – isocyanate index (II) on the processing and performance properties of composites was examined. Chemical and cellular structure, as well as mechanical and thermal properties of the resulting environmental-friendly composites were examined.

2 Experimental

2.1 Materials

Rigid PUR-PIR foams were synthesized from CG a bio-based polyol prepared according to the patent application developed at the Department of Polymer Technology of Gdańsk University of Technology (21) and commercially available polyols from the PCC Rokita, Poland, Rokopol G441 (trifunctional polyether based on glycerol) and Rokopol RF55 (high functional polyether based on sorbitol). Biopolyol CG was as synthesized from crude glycerol and castor oil during a two-step process comprising crude glycerol polycondensation and a further reaction with castor oil. Synthesis of CG biopolyol was described in more detail in our previous work (2). The properties of the aforementioned polyols are presented in Table 1.

Table 1: Properties of polyols used during foams' preparation.

Property	Polyol		
	CG	Rokopol G441	Rokopol RF55
Density (g/cm^3)	1.18	1.07	1.09
Hydroxyl number (mg KOH/g)	460	345	495
Viscosity (mPas)	1300	280	9200
Water content (wt.%)	0.207	<0.100	<0.100

Isocyanate used in the reaction was polymeric 4,4′-methylene diphenyl diisocyanate (pMDI) characterized by a 31.5% content of NCO groups, obtained from Borsodchem, Hungary. The average functionality of pMDI was ca. 2.8.

Fyrol PNX produced by ICL Industrial Products was used as a flame retardant. Two types of tertiary amines (DABCO 1027 and DABCO TMR-2) were applied as catalysts. Both were purchased from Air Products and Chemicals, Inc., USA, Tegostab B 8465 from Evonik Industries, Germany and were used as silicon-based surfactants. The physical blowing agent was liquid hydrofluorocarbon blend Solkane® 365/227 from Solvay, Belgium. Distilled water was used as a chemical blowing agent.

BSG was provided by Energetyka Złoczew sp. ZOO, Poland. It resulted from production of light lager and consisted only of barley malts, only pilsner malt. Generally, BSG resulting from mashing process is similar, in its appearance, to ground grain and contains a lot of water. The color and amount of husk depends on the malts used to produce beer, our BSG contained a noticeable amount of husk and it was light brown in color. In the presented research work, we dried BSG at 80°C in order to significantly decrease the moisture content. As the size of the filler particles has significant influence on the final distribution of the filler in polymer matrix and the properties of resulting composite, prior to processing, BSG was mechanically ground in a co-rotating twin-screw extruder at 120°C to obtain particles with a narrow size distribution. Among other methods of comminution, extrusion was investigated by Caprez et al. (22) in terms of its influence on the chemical composition of wheat bran. Parameters of the process were similar to those applied in the presented study – temperature 100°C, screw speed 100 rpm. The authors proved that modification of bran by extrusion had an insignificant impact on its chemical composition. Because of the similarity in chemical composition it can be assumed that same phenomenon occurs for BSG.

2.2 Preparation of PUR-PIR foams

Rigid PUR-PIR foams were produced on a laboratory scale by a single step method from a two-component (A and B) system with the ratio of NCO/OH groups of 1.5, 2.0 and 2.5. Samples were coded as II150, II200 and II300 according to used isocyanate index.

Component A (polyol mixture) consisting of the proper amounts of Rokopol RF55, biopolyol CG or their mixtures with oligoether Rokopol G441 at various ratios, flame retardant, catalysts, surfactant, foaming agents and filler was weighed and placed in a 500 ml polypropylene

cup. Next, the polyol mixture was homogenized with a mechanical stirrer at 2000 rpm for 60 s. Such prepared component A was mixed with component B (pMDI) at a predetermined mass ratio and stirred at 2000 rpm for 20 s. The resulting reaction mixture was left in cup for a free rise. Obtained samples were conditioned at room temperature for 24 h. Table 2 contains the details of the foams' formulations.

2.3 Characterization

Elemental analysis (C, H, N, S) of BSG was carried out using a Flash 2000 CHNSO Analyzer from Thermo Scientific (USA).

Particle size distribution of cellulosic filler was determined by sieve analysis according to our internal laboratory standard. Approximately 100 g of filler was manually sieved in constant time (30 min), using woven wire cloth sieves with sizes 1.02, 0.75, 0.50, 0.25 and 0.12 mm, respectively.

Fourier transform infrared (FTIR) spectrophotometric analysis of biofiller and rigid foams was performed in order to determine their chemical structure. The analysis was performed at a resolution of 4 cm^{-1} in the range 650–4000 cm^{-1} (64 scans) using a Nicolet Spectrometer IR200 spectrometer (Thermo Scientific, USA) equipped with a diamond crystal.

Reaction kinetics of PUR-PIR composite foams were evaluated by analyzing the temperature during preparation. After pouring the reaction mixture into the polypropylene cup, the temperature inside the foam was measured by a thermocouple placed in the cup.

Table 2: Formulations of prepared foams.

Raw materials (pbw)	Foam symbol		
	II150	II200	II300
Rokopol RF55	30.0	30.0	30.0
Rokopol G441	35.0	35.0	35.0
Biopolyol CG	35.0	35.0	35.0
Fyrol PNX	25.0	25.0	25.0
DABCO 1027	1.5	1.5	1.5
DABCO TMR-2	1.0	1.5	1.5
Tegostab B 8465	2.0	2.0	2.0
Solkane	30.0	40.0	50.0
Water	0.5	0.5	0.5
BSG	65.3	78.5	91.7
Isocyanate	166.7	222.3	277.9
Isocyanate index	150	200	250
Content of bio-polyol in foam, wt.%	8.9	7.4	6.4
Content of bio-based material in foam, wt.%	25.6	24.1	23.0

After conditioning, foams were cut into samples whose properties were later determined in accordance with the standard procedures.

The apparent density of samples was calculated in accordance with PN-EN ISO 845:2000, as a ratio of the sample weight to the sample volume (g/cm^3). The cylindric samples were measured with a slide caliper with an accuracy of 0.1 mm and weighed using electronic analytical balance with an accuracy of 0.0001 g.

Swelling degree and sol fraction were determined during the swelling test. Samples of PUR-PIR foams (around 0.2 g) were swollen in xylene for 72 h (room temperature). The swelling degree was calculated in accordance with equation 1:

$$Q = \frac{m_{72h} - m_o}{m_o} \times 100\% \quad [1]$$

where: Q – swelling degree (%), m_t – mass of the sample swollen after 72 h (g), m_o – initial mass of sample (g).

Sol fraction was calculated as mass difference of biocomposites before swelling (W_1) and after extraction (W_2), according to equation 2:

$$\text{Sol fraction} = \frac{W_1 - W_2}{W_1} \times 100\% \quad [2]$$

The morphology of the samples was evaluated by using a Hitachi model S3400 (Hitachi, Japan) scanning electron microscopy.

The compressive strength of rigid foams was estimated basing on the EN ISO 844:2007 standard. The cylindric samples with dimensions of 20×20 mm (height and diameter) were measured with a slide caliper with an accuracy of 0.1 mm. The compression test was performed on a Zwick/Roell (Germany) tensile tester at a constant speed of 10%/min until reaching 20% deformation.

Dynamic mechanical analysis was performed using a DMA Q800 TA Instruments (USA) apparatus. Samples were analyzed in the compression mode with a frequency of 1 Hz. Measurements were performed for the temperature range from 25°C to 250°C with a heating rate 4°C/min. Samples were cylindrically-shaped with dimensions of 8×12 mm.

The thermal analysis of samples was performed using the thermogravimetric analyzer model Q600 from TA Instruments (USA). Samples weighing approx. 4 mg were placed in a corundum dish. The study was conducted in an inert gas atmosphere – nitrogen (flow rate of 100 ml/min) in the temperature range from 25°C to 700°C with a temperature increase rate of 20°C/min. Volatile products from thermal degradation of samples were also evaluated using a FTIR spectroscopy using a Nicolet iS10 spectrometer from Thermo Scientific (USA).

Table 3: Properties of used BSG biofiller.

Method	Element	Element content, wt.%	Method	$TCI_{1371/2900\ cm^{-1}}$	$LOI_{1430/893\ cm^{-1}}$	$HBI_{3336/1336\ cm^{-1}}$
Elemental analysis	C	47.70	FTIR	1.16	0.89	1.33
	H	5.15				
	N	3.37				

3 Results and discussion

3.1 Properties of BSG biofiller

In Table 3 there are shown characteristics of BSG filler determined by elemental analysis and FTIR spectroscopy. BSG was characterized with a relatively high content of nitrogen compared to other cellulosic biofillers commonly used in the manufacturing of polymer composites (23). Such a phenomenon was related to the noticeably higher protein content of BSG, which was repeatedly proven in the literature (14, 24). Moreover, applied BSG was generated from lager production, which results in higher protein content compared to BSG from the brewing of ale type beer (25).

Figure 1 presents FTIR spectra of the applied BSG filler. The absorption band (A) characteristic for the stretching vibrations of O-H bonds was observed in the range of 3300–3350 cm^{-1}. Signals at 2925 and 2849 cm^{-1} (B) were attributed to the symmetric and asymmetric stretching vibrations of C-H bonds. Peak (C) at 1745 cm^{-1} is characteristic for the ester groups between hydroxycinnamic acids present in BSG and lignin or hemicellulose (26). Signal (D) around 1640 cm^{-1} can be associated with the presence of C=C bonds conjugated with C=O bonds and their stretching vibrations. Band (E) at 1523 cm^{-1} represents C=C bonds in the aromatic rings of lignin (27). Multiplet peaks (F) characteristic for deformation vibrations of C-H and O-H bonds were observed around 1450 cm^{-1}. Signals (G) observed in the range of 1230–1240 cm^{-1} were attributed to the presence of C-O and C=O bonds and their stretching vibrations (28). Also bands (H) at 1145–1155 cm^{-1} and 1020–1030 cm^{-1} can be associated with vibrations of C-O bonds. Low intensity signals (i) around 890 and 850 cm^{-1} characteristic for antisymmetric out-of-phase ring stretching in the carbohydrate structure of used BSG were observed (29).

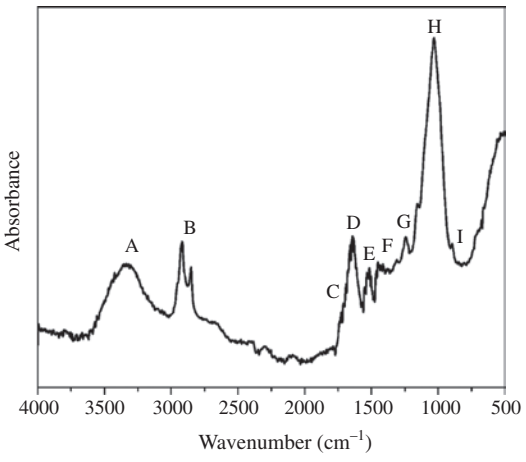

Figure 1: FTIR spectra of the used BSG filler.

It should also be mentioned, that proteins, present in significant amounts in BSG, might have an important impact on the intensity of the bands in the FTIR spectra. Such an effect is related to similar positions of infrared bands characteristic for cellulose and proteins (30). For example, very characteristic peaks for stretching vibrations of N-H groups around 3300 cm^{-1} are overlap with peaks for O-H groups. Signals around 1640 cm^{-1}, attributed to the vibrations of C=C and C=O bonds might be enhanced by the contribution of out-of-phase C-N stretching vibration, the C-C-N deformation and the N-H in-plane bending. Moreover, the presence of proteins in BSG increases the possibility of hydrogen bonding, which may cause noticeable shifts of absorption bands.

FTIR analysis was also used to determine the crystallinity of applied BSG filler. Factors describing crystallinity, such as the total crystallinity index ($TCI_{1371/2900\ cm^{-1}}$), lateral order index ($LOI_{1430/893\ cm^{-1}}$) and hydrogen bond intensity ($HBI_{3336/1336\ cm^{-1}}$) were calculated from the absorption ratios at proper wavenumbers, as proposed by Kljun et al. (31). The LOI parameter is associated with the overall degree of alignment in the cellulose, while hydrogen bond intensity (HBI) is related to the crystal system and the degree of intermolecular regularity, as well as the amount of bound water. Calculated values of TCI and LOI are similar to those presented in other research work for biofillers such as wood flour or wheat bran (23, 31). However, the value of HBI was noticeably higher, which can be related to the moisture content of BSG (0.52 wt.%) and presence of proteins, which, as mentioned above, increase the possibility of hydrogen bonding.

Table 4 presents the particle size distribution of the used filler. The size of filler particles can have a significant influence on the performance of the composite, as it

Table 4: Particle size distribution of BSG filler.

Particle size (mm)	Percentage content (wt.%)
>1.02	0.08
0.76–1.02	2.13
0.51–0.75	2.87
0.26–0.50	32.59
0.12–0.25	47.78
<0.12	12.54

affects the dispersibility in the polymer matrix. As could be observed, the mix of particles with various sizes were used during the preparation of PUR-PIR foams. For both types of BSG almost 95 wt.% of particles were smaller than 0.50 mm, which confirms that co-rotating twin screw extrusion can be considered as an efficient grinding method for cellulosic fillers.

3.2 Properties of rigid PUR-PIR foams

Except the main reaction resulting in the generation of urethane groups in the material, isocyanates undergo various side reactions, which contribute to the enhanced crosslinking of foams. Figure 2 presents the general schemes of these reactions. Obviously, the increase of the isocyanate index leads to the increasing intensity of the side reactions, simultaneously promoting the formation of trifunctional species contributing to the total crosslink density, such as in allophanate, biuret or isocyanaurate groups. Moreover, the use of water as a chemical blowing agent intensifies the generation of urea and, at the end, the biuret groups. It is worth mentioning that the formation of biuret is significantly faster than the formation of allophanate, therefore the application of water in PUR systems has a very big impact on crosslink density of the material (32).

Figure 3 shows the plots of temperature as a function of time during the preparation of rigid foams. A noticeable decrease of reaction temperature was observed. Such a phenomenon was associated with the significant increase of the physical blowing agent required to provide the same apparent density with the rise of the isocyanate index (see Table 2). Moreover, the thermal effect of side reactions occurring at higher isocyanate indexes is lower than the reaction between polyol and isocyanate, e.g. enthalpy of reaction (ΔH) for trimerization is around 80 kJ/kmol, while for generation of urethane groups it exceeds 105 kJ/kmol (33, 34). From the presented temperature curves it can also be seen that the increase of the isocyanate index resulted in the retardation of foaming and polymerization, which confirms the results presented in other works (32).

Table 5 presents the properties of the prepared polyurethane composites. The apparent density obviously has a great impact on the performance of the foamed materials. Formulations of foams were developed (varying the amount of physical blowing agent Solkane 365/227) in order to provide a similar density for all investigated materials at the level of 51 ± 2 kg/m^3. It can be seen (Table 2) that the amount of hydrofluorocarbon foaming agent necessary to provide the same level of volumetric expansion during the manufacturing of foam, thus the same density, increased with isocyanate index.

Table 5 also presents the results of the swelling tests. The swelling degree the decreases with the increase of the isocyanate index. Simultaneously, the decrease of the sol fraction was observed, which points to the increasing crosslink density of the material. Such a phenomenon related to the increasing isocyanate index was also observed by other researchers (35).

Table 5 also presents the values of the average cell size of the investigated foams and Figure 4 presents the SEM micrographs of the prepared foams. It can be seen that the increase of the isocyanate index resulted in the decrease of the average cell size from 200 to 159 μm. Such a phenomenon can be associated with the increasing crosslink density of the material and the stiffening of the cell walls, due to the intensification of the allophanate and biuret groups formation, which impeded the growth of cells (32). As can be seen in presented images, the shape of cells was hardly affected by changes in the foams' formulation.

Stiffness of the foamed material during compression arises from the buckling of the cell walls, so its compressive performance is strongly correlated with cellular structure and its packaging (9). Therefore, the apparent density is a very important parameter of the foamed material when discussing its compressive performance. That was one of the reasons why composites were prepared with similar density. Table 6 presents the values of the compressive strength of the investigated rigid PUR-PIR foamed composites. It can be seen that isocyanate index did not have a significant impact on the strength of the material. Deterioration of compressive strength parallel to the foaming direction was observed. Such a phenomenon can be associated with the increase of the foams' friability with the increase of the isocyanate index (36). Similar results, pointing to deterioration of the compressive performance with the increase of isocyanate index were observed by other researchers (35, 37).

Figure 5 presents the plots of loss tangent (tan δ) as a function of temperature for the prepared samples. As

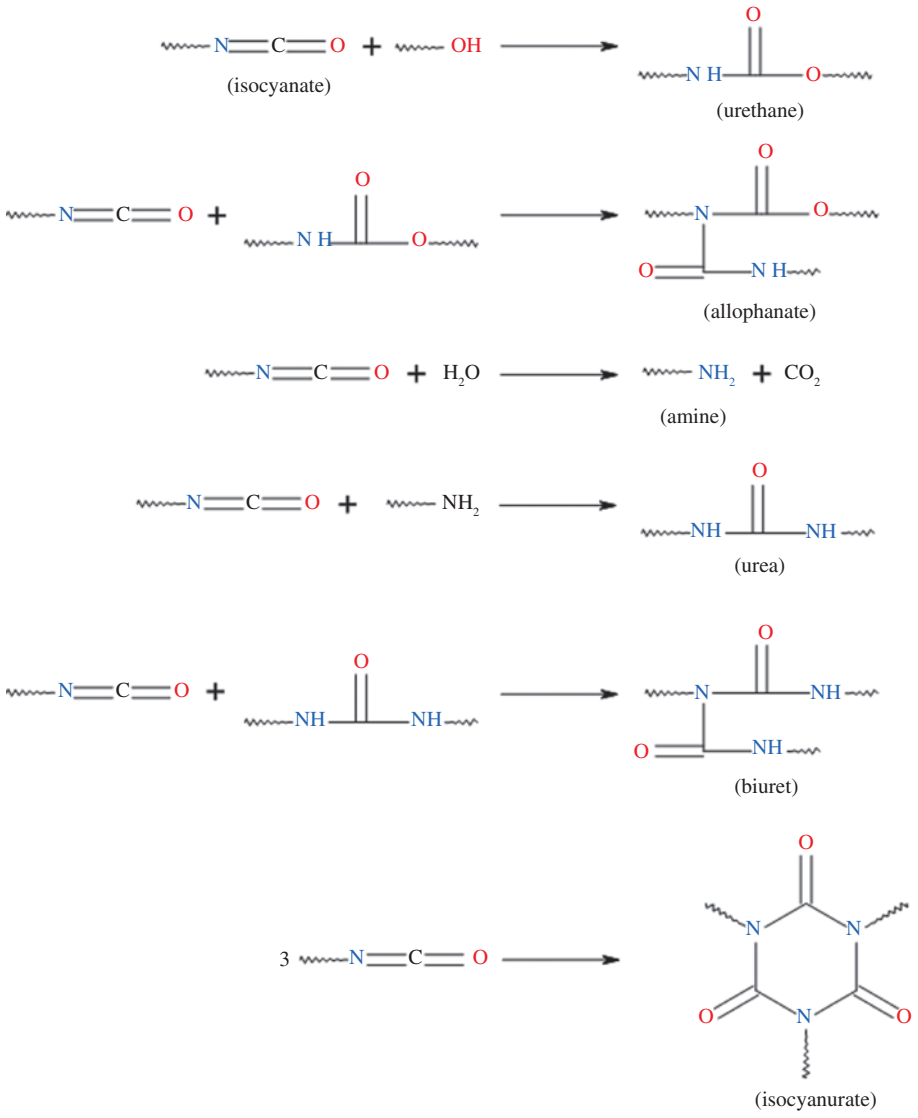

Figure 2: Main reactions occurring during the preparation of polyurethane foams.

the isocyanate index increased, the temperature position of the maximum value of tan δ peak was shifted towards higher temperatures. The position of these peaks is generally used to determine the glass transition temperature (T_g) of materials. As expected, the increase of the isocyanate index resulted in the significant rise of T_g. As mentioned already, such a phenomenon is strictly associated with the side reactions of the isocyanate groups, which lead to the formation of trifunctional allophanate and biuret groups, simultaneously increasing the stiffness of polyurethane. Increase of the isocyanate index from 150 to 200 and 250 shifted T_g by 23.5 and 27.5°C.

Except for the temperature shift of the tan δ peak, some changes in its magnitude can be observed, which is related to the nature of the polymer matrix. Low values of tan δ indicate the higher elasticity of the material, while higher values characterize materials with a high, non-elastic strain component. The latter group is able to dissipate a higher amount of energy by various molecular motions (38). It can be seen that an increase of the isocyanate index resulted in the slight enhancement of the magnitude of the tan δ peak. It points to higher energy dissipation, in this case related to the cracking of crosslinks comprised of allophanate, biuret and isocyanaurate groups, whose presence increase the friability of foams.

The FTIR spectra of the produced foams are presented in Figure 6. The absorption band characteristic for stretching vibrations of N-H groups (in urethane bonds) was observed in the range 3296–3308 cm^{-1}. Signals associated with the bending vibrations of these groups were

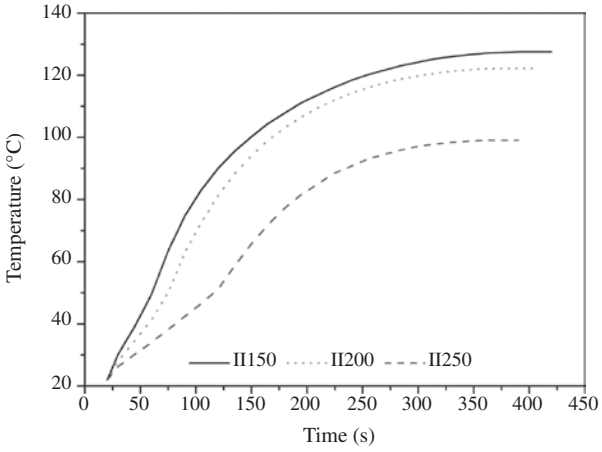

Figure 3: Temperature during synthesis as a function of time for the prepared foams.

Table 5: Comparison of the foams' properties.

Properties	Foam symbol		
	II150	II200	II250
Apparent density (kg/m³)	50.0 ± 1.0	51.6 ± 2.4	52.8 ± 2.0
Swelling degree (wt.%)	384 ± 1	313 ± 7	326 ± 2
Sol fraction (wt.%)	8.9 ± 1.2	7.3 ± 1.2	6.3 ± 1.3
Average cell size (μm)	200 ± 30	178 ± 26	159 ± 19

observed at 1509–1513 cm^{-1} (39). The absorption maxima around 1715 cm^{-1} corresponded to the stretching vibrations of C=O bonds. Bands at 1213–1215 cm^{-1} were attributed to the stretching vibrations of C-N bonds in urethane linkages (40). The aforementioned signals confirm the presence of urethane bonds in the analyzed foams. Bands at 2858–2870 and 2922–2927 cm^{-1}, characteristic for symmetric and asymmetric stretching vibrations of C-H bonds in CH_2 groups were present in aliphatic chains and CH_3 end groups were observed. Peaks at 2272–2277 cm^{-1} resulted from the presence of unreacted -N=C=O groups, due to the excess of isocyanate used in the synthesis of the foams (41). It can be seen that the magnitude of these peaks increases with the rise of the isocyanate index. Around 1594 cm^{-1}, peaks associated with the presence of aromatic groups in the material, mainly in applied biofillers were observe. Signals at 1411–1412 cm^{-1} were assigned to the presence of isocyanurate rings, products of the isocyanate trimerization (42). Multiplet bands in the range of 1017–1070 cm^{-1} were associated with the presence of δ bonds between carbon and oxygen atoms (in the case of ether bonds), which is related to the structure of the polyols used (43).

Table 7 presents the results of thermogravimetric analysis of the prepared rigid foams. As expected, the increase of the isocyanate value enhanced the thermal stability of the material, which confirms the results obtained by other researchers (44). Noticeable, a 15°C rise of temperature of degradation onset (related to the decomposition of 2 wt.% of foam) was observed, when the isocyanate index was increased from 150 to 250. Such a phenomenon was related to the increased amount of isocyanurate rings present in the foams, which are products of the isocyanate group trimerization (as presented in Figure 2).

Figure 7 shows the differential thermogravimetric curves (DTG) plotted for the prepared PUR-PIR foams. It can be seen that for all samples thermal decomposition shows a similar pathway. Despite that only one significant peak on the curves is observed, thermal degradation can be divided into four stages, but the peaks related to these stages are overlapping. The first one (A), occurring in the range of 200–235°C is related to the evaporation and decomposition of less thermally stable additives. For example, according to the data sheet, Fyrol PNX shows a 5 wt.% mass loss around 215°C. Moreover, thermal degradation of biopolyol CG also starts around 200–210°C. Subsequently (B), decomposition of the weaker bonds such as biuret, allophanate and urethane, occurs resulting in the generation of carbon dioxide and various transition components (45). Also, the backbone of Rokopol G441 starts to degrade around 320°C. Around 360°C (C) the decomposition of soft segments comprised of Rokopol RF55 occurs. Moreover, the second step of biopolyol CG degradation is observed around 380–400°C, which is associated with the castor oil used during the biopolyol synthesis (46). At higher temperatures (D), thermolysis of the residues from former degradation steps takes place (47). It can be clearly seen that the decomposition of soft segments is noticeably slower than the decomposition of rigid ones, comprised of thermally less stable bonds (48).

TGA-FTIR analysis was performed in order to investigate the gas products of the thermal decomposition of the prepared rigid foams. Figure 8 shows the FTIR spectra of the foams' decomposition products. Generally, all the foams showed very similar spectra. The noises in the range of 3400–4000 cm^{-1} and 1250–2150 cm^{-1} are related to the water vapor generated during the thermal decomposition of the foamed composites. All absorption maxima were attributed to proper bonds, their vibrations and degradation products of polyurethanes and are summarized in Table 8. Multiplet peaks associated with the presence of hydrocarbons in analyzed gases were observed in the range of 2880–2980 cm^{-1}. These peaks were attributed to the symmetric and asymmetric stretching vibrations

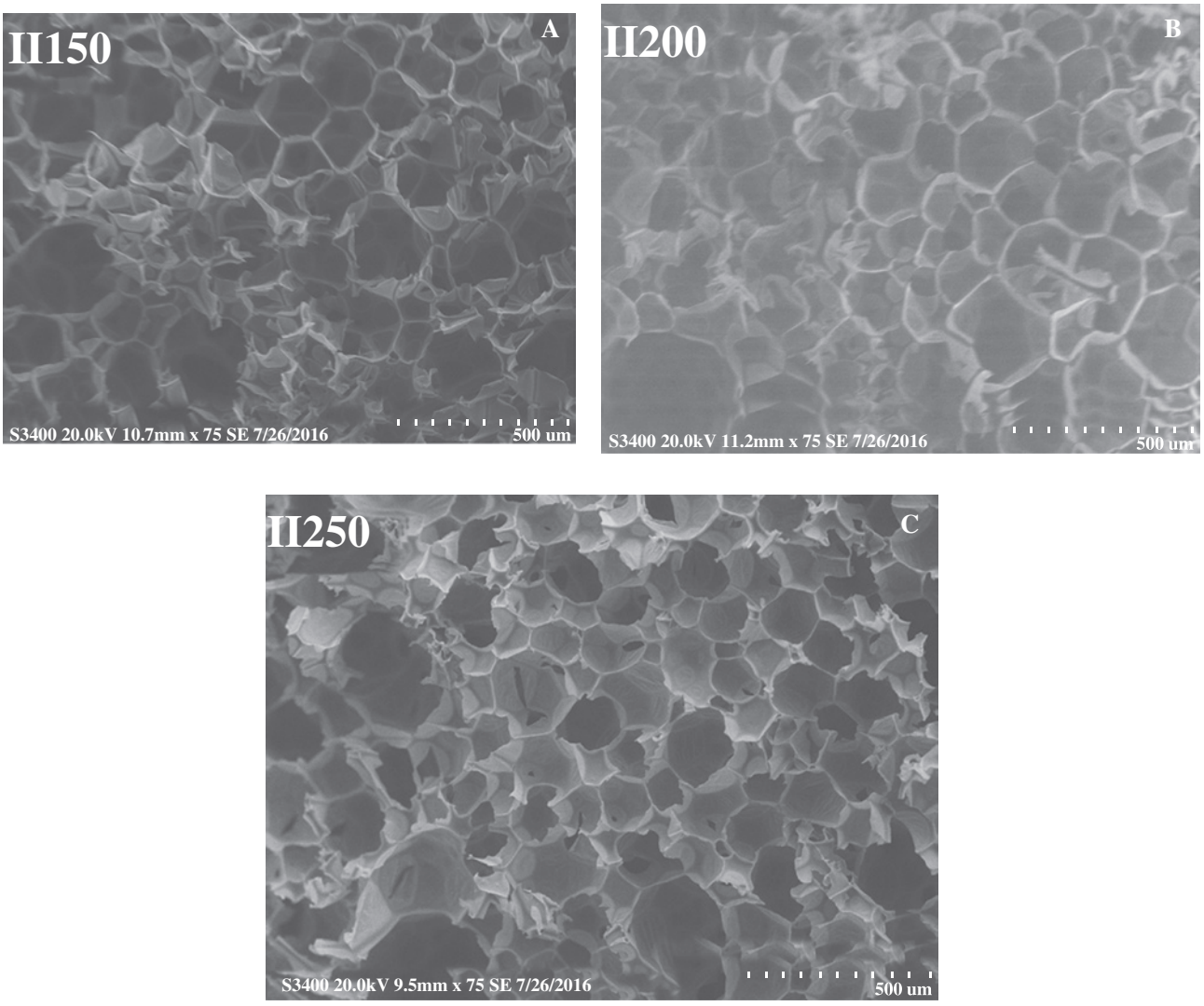

Figure 4: SEM images of II150, II200 and II250 foams.

Table 6: Compressive performance of the prepared composites.

Foam symbol	Compressive strength (kPa)		Anisotropy (%)
	Parallel to foam rise	Perpendicular to foam rise	
II150	226±19	158±8	43
II200	214±5	156±5	37
II250	202±8	160±10	26

of C-H bonds in CH_2 groups present in aliphatic chains and CH_3 end groups. Signals observed in the range of 2245–2385 cm^{-1} were obtained by the overlapping of various maxima associated with the stretching of N-H bonds present in amines, C-O bonds in carbon monoxide and dioxide, C-N bonds in nitriles and hydrogen cyanide

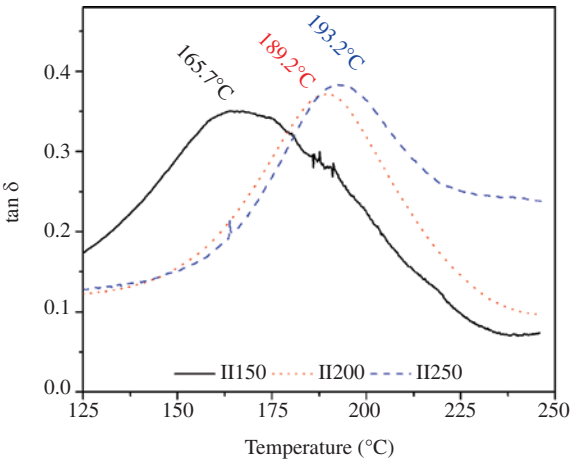

Figure 5: Plots of loss tangent as a function of temperature for the prepared rigid foams.

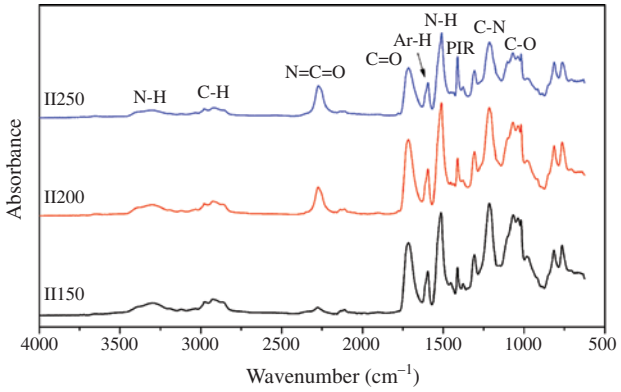

Figure 6: FTIR spectra of the prepared rigid PUR-PIR/BSG composites.

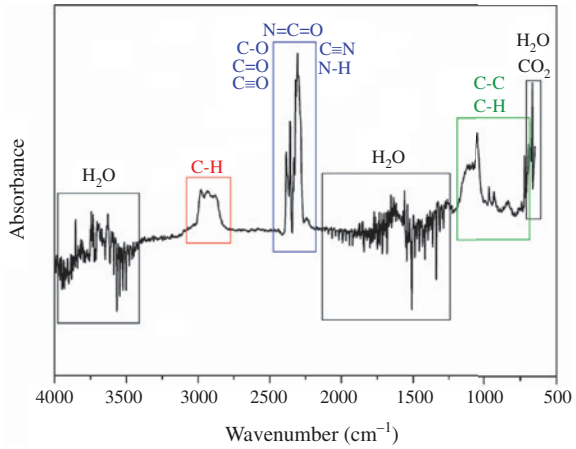

Figure 8: FTIR spectra of the foams' decomposition products.

Table 7: Characteristics of thermal degradation of rigid PUR-PIR foams.

Sample	Mass loss (%)			
	2	5	10	50
	Temperature (°C)			
II150	196.0	231.2	260.7	362.8
II200	201.7	233.6	266.5	382.5
II250	211.0	243.1	268.7	381.1

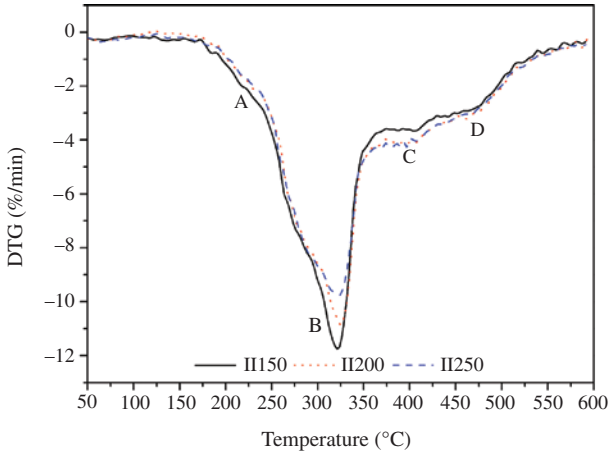

Figure 7: DTG curves for the prepared foams.

and NCO groups of the used isocyanate. Various bands, including multiplet ones, associated with the presence of aliphatic and aromatic hydrocarbons generated during thermal decomposition of rigid polyurethane foams were observed at wavenumbers lower than 1125 cm^{-1}. Around 670 and 740 cm^{-1} signals characteristic for the bending vibrations of CO_2 particle and libration of H_2O particle, respectively, were observed (49).

4 Conclusions

Rigid polyurethane-polyisocyanurate composite foams were prepared by the incorporation of BSG into the foamed matrix. Around 16.7 wt.% of BSG was introduced into the PUR/PIR composition. The influence of the isocyanate index (from 150 to 250) on properties of such materials was evaluated. The results presented indicate that the rise of the isocyanate index caused the increase of the amount of the physical blowing agent required to provide a similar level of the material's apparent density. Moreover, the increase of the isocyanate index intensified the generation of allophanate and biuret groups and isocyanurate rings in the material, which resulted in the higher crosslink density of the material confirmed by the swelling tests and dynamic mechanical analysis. The other effect of the enhanced generation of the functional groups mentioned above is the stiffening of cell walls, which caused a slight decrease of cell size of the prepared biocomposites from 200 to 159 µm. Compressive performance of material was deteriorated by 23%, which can be associated with the increased friability of highly crosslinked cellular structure of PUR-PIR foams. Moreover, enhanced generation of isocyanurate rings, confirmed by FTIR analysis, resulted in the delay of thermal decomposition by 15°C, which can be considered very beneficial from the point of safety. However, changes in the isocyanate index did not have noticeable impact on the amount and type of products of thermal degradation of analyzed biocomposites.

Summarizing, this work confirms that BSG can be successfully used to prepare foamed PUR-PIR composites. Such a solution may be considered very eco-friendly and

Table 8: Detailed analysis of the TG-FTIR spectra of the prepared rigid foams.

Wavenumber (cm^{-1})	Bond (vibration)	Degradation product
2977	C-H (asymmetric stretching)	C_xH_y
2941	C-H (asymmetric stretching)	C_xH_y
2883	C-H (symmetric stretching)	C_xH_y
2385	N-H (asymmetric stretching)	$R\text{-}NH_2$
2354	N-H (asymmetric stretching) and C-O (stretching)	$R\text{-}NH_2$, CO, CO_2
2307	C-N (stretching) and NCO (asymmetric stretching)	R-CN, R-NCO
2245	C-N (stretching)	R-CN
1125	C-H (deformation)	C_xH_y
1047	C-H (in-plane bending)	C_xH_y
963	C-C (skeletal) and CH_3 (rocking)	C_xH_y
927	C-C (skeletal) and CH_3 (rocking)	C_xH_y
839	C-C (skeletal)	C_xH_y
740	H_2O (libration) and C-H (out-of-plane bending)	H_2O, C_xH_y
670	O=C=O (bending)	CO_2

obviously beneficial from the economical point of view, due to the utilization of low-cost waste cellulosic filler. Moreover, the results obtained and the present state-of-the-art indicate that further studies on that field should focus on: (i) the evaluation of the type of BSG filler on the performance of PUR-PIR foamed composites; (ii) the analysis of biodegradation of prepared green composites; (iii) the analysis of the BSG impact on the thermal insulation properties of foams and their changes during long time storage of the material.

References

1. Piszczyk Ł, Strankowski M, Danowska M, Hejna A, Haponiuk JT. Rigid polyurethane foams from a polyglycerol-based polyol. Eur Polym J. 2014;57:143–50.
2. Hejna A, Kirpluks M, Kosmela P, Cabulis U, Haponiuk JT, Piszczyk Ł. The influence of crude glycerol and castor oil-based polyol on the structure and performance of rigid polyurethane-polyisocyanurate foams. Ind Crop Prod. 2017;95:113–25.
3. Piszczyk Ł, Hejna A, Formela K, Danowska M, Strankowski M. Effect of ground tire rubber on structural, mechanical and thermal properties of flexible polyurethane foams. Iran Polym J. 2015;24:75–84.
4. Piszczyk Ł, Hejna A, Formela K, Danowska M, Strankowski M. Rigid polyurethane foams modified with ground tire rubber – mechanical, morphological and thermal studies. Cell Polym. 2015;2:45–62.
5. Piszczyk Ł, Hejna A, Danowska M, Strankowski M, Formela K. Polyurethane/ground tire rubber composite foams based on polyglycerol: processing, mechanical and thermal properties. J Reinf Plast Comp. 2015;34:708–17.
6. Hejna A, Kopczyńska M, Kozłowska U, Klein M, Kosmela P, Piszczyk Ł. Foamed polyurethane composites with different types of ash – morphological, mechanical and thermal behavior assessments, Cell Polym. 2016;35(6):287–308.
7. Kurańska M, Prociak A, Kirpluks M, Cabulis U. Porous polyurethane composites based on bio-components. Compos Sci Technol. 2013;75:70–6.
8. Casado U, Marcovich NE, Aranguren MI, Mosiewicki MA. High-strength composites based on tung oil polyurethane and wood flour: effect of the filler concentration on the mechanical properties. Polym Eng Sci. 2009;49:713–21.
9. Mosiewicki MA, Dell'Arciprete GA, Aranguren MI, Marcovich NE. Polyurethane foams obtained from castor oil-based polyol and filled with wood flour. J Compos Mater. 2009;43:3057–72.
10. Kurańska M, Prociak A. Porous polyurethane composites with natural fibres. Compos Sci Technol. 2012;72:299–304.
11. Li Y, Ren H, Ragauskas AJ. Rigid polyurethane foam/cellulose whisker nanocomposites: preparation, characterization, and properties. J Nanosci Nanotechnol. 2011;11(8):6904–11.
12. Czupryński B, Liszkowska J, Paciorek-Sadowska J. Effect of selected boroorganic compounds and fillers on thermal properties of rigid polyurethane-polyisocyanurate foams. J Polym Eng. 2006;26(6):589–604.
13. Paciorek-Sadowska J, Czupryński B, Liszkowska J. Application of waste products from agricultural-food industry for production of rigid polyurethane-polyisocyanurate foams. J Porous Mat. 2011;18:631–8.
14. Mussatto SI, Dragone G, Roberto IC. Brewers' spent grain: generation, characteristics and potential applications. J Cereal Sci. 2006;43:1–14.
15. The Brewers of Europe, 2012. Beer statistics 2012 edition. 16 Nov. 2012. Web. 1 Aug. 2014.
16. Mussatto SI, Roberto IC. Chemical characterization and liberation of pentose sugars from brewer's spent grain. J Chem Technol Biotechnol. 2006;81:268–74.
17. Ktenioudaki A, Chaurin V, Reis SF, Gallagher E. Brewer's spent grain as a functional ingredient for breadsticks. Int J Food Sci Tech. 2012;47:1765–71.
18. Russ W, Mortel H, Pittroff RM. Application of spent grains to increase porosity in bricks. Construct Build Mat. 2005;19(2):117–26.
19. Hashemi M, Razavi SH, Shojaosadati SA, Mousavi SM. The potential of brewer's spent grain to improve the production of

α-amylase by Bacillus sp. KR-8104 in submerged fermentation system. New Biotechnol. 2011;28:165–72.
20. Mussatto SI, Fernandes M, Dragone G, Mancilha IM, Roberto IC. Brewer's spent grain as raw material for lactic acid production by Lactobacillus delbrueckii. Biotechnol Lett. 2007;29:1973–6.
21. Haponiuk JT, Piszczyk Ł, Danowska M, Strankowski M. Sposób wytwarzania ekologicznych polioli z odpadu do transestryfikacji olejów roślinnych oraz sposób wytwarzania sztywnych pianek poliuretenowych. Patent application P. 408610, 2014.
22. Caprez A, Arrigoni E, Amadò R, Neukom H. Influence of different types of thermal treatment on the chemical composition and physical properties of wheat bran. J Cereal Sci. 1986;4:233–9.
23. Formela K, Hejna A, Piszczyk Ł, Reza Saeb M, Colom X. Processing and structure-property relationships of natural rubber/wheat bran biocomposites. Cellulose. 2016;23(5):3157–75.
24. Tang D, Yin G, He Y, Hu S, Li B, Li L, Liang H, Borthakur D. Recovery of protein from brewer's spent grain by ultrafiltration. Biochem Eng J. 2009;48:1–5.
25. Robertson JAI, Anson KJA, Treimo J, Faulds CB, Brocklehurst TF, Eijsink VGH, Waldron KW. Profiling brewers' spent grain for composition and microbial ecology at the site of production. LWT Food Sci Technol. 2010;43:890–6.
26. Sun XF, Xu F, Sun RC, Geng ZC, Fowler P, Baird MS. Characteristics of degraded hemicellulosic polymers obtained from steam exploded wheat straw. Carbohyd Polym. 2005;60(1):15–26.
27. Colom X, Carrillo F, Nogues F, Garriga P. Structural analysis of photodegraded wood by means of FTIR spectroscopy. Polym Degrad Stab. 2003;80:543–9.
28. dos Santos DM, Bukzem AL, Ascheri DPR, Signini R, de Aquino GLB. Microwave-assisted carboxymethylation of cellulose extracted from brewer's spent grain. Carbohyd Polym. 2015;131:125–33.
29. Alemdar A, Sain M. Isolation and characterization of nanofibers from agricultural residues – wheat straw and soy hulls. Bioresource Technol. 2008;99(6):1664–71.
30. Barth A. Infrared spectroscopy of proteins. Biochim Biophys Acta (BBA)-Bioenerg. 2007;1767:1073–101.
31. Kljun A, Benians TAS, Goubet F, Meulewaeter F, Knox JP, Blackburn RS. Comparative analysis of crystallinity changes in cellulose I polymers using ATR-FTIR, X-ray diffraction, and carbohydrate-binding module probes. Biomacromolecules. 2011;12:4121–6.
32. Dusek K, Spirkova M, Havlicek I. Network formation of polyurethanes due to side reactions. Macromolecules. 1990;23(6):1774–81.
33. Bykova TA, Lebedev BV, Kiparisova EG, Tarasov EN, Frenkel TM, Pankratov VA, Vinogradova SV, Korshank VV. Thermodynamics of phenyl isocyanate, the process of its cyclotrimerization, and the triphenyl isocyanurate that is formed, in the 0–330°K interval. J Gen Chem USSR. 1985;55:2303–8.
34. Lovering EG, Laidler KJ. Thermochemical studies of some alcohol-isocyanate reactions. Can J Chem. 1962;40:26–30.
35. Kim SH, Kim BK. Effect of isocyanate index on the properties of rigid polyurethane foams blown by HFC 365mfc. Macromol Res. 2008;16(5):467–72.
36. Modesti M, Lorenzetti A. An experimental method for evaluating isocyanate conversion and trimer formation in polyisocyanate-polyurethane foams. Eur Polym J. 2001;37(5):949–54.
37. Stirna U, Sevastyanova I, Misane M, Cabulis U, Beverte I. Structure properties of polyurethane foams obtained from rapeseed oil polyols. Proc Estonian Acad Sci Chem. 2006;55(2):101–10.
38. Bindu P, Thomas S. Viscoelastic behavior and reinforcement mechanism in rubber nanocomposites in the vicinity of spherical nanoparticles. J Phys Chem B. 2013;117:12632–48.
39. Sormana JL, Meredith JC. High-throughput discovery of structure-mechanical property relationships for segmented poly(urethane-urea)s. Macromolecules. 2004;37:2186–95.
40. Fournier D, Du Prez F. "Click" chemistry as a promising tool for side-chain functionalization of polyurethanes. Macromolecules. 2008;41:4622–30.
41. Jiao L, Xiao H, Wang Q, Sun J. Thermal degradation characteristics ofrigid polyurethane foam and the volatile products analysis with TG-FTIR-MS. Polym Degrad Stab. 2013;98:2687–96.
42. Samborska-Skowron R, Balas A. Qualitative identification of isocyanurate rings in urethane-isocyanurate elastomers and their hydrolyzates (in Polish). Polimery 2003;48:371–4.
43. Pretsch T, Jakob I, Müller W. Hydrolytic degradation and functional stability of a segmented shape memory poly(ester urethane). Polym Degrad Stab. 2009;94(1):61–73.
44. Kurańska M, Prociak A, Kirpluks M, Cabulis U. Polyurethane-polyisocyanurate foams modified with hydroxyl derivatives of rapeseed oil. Ind Crop Prod. 2015;74:849–57.
45. Tanaka R, Hirose S, Hatakeyama H. Preparation and characterization of polyurethane foams using a palm oil-based polyol. Bioresource Technol. 2008;99:3810–6.
46. Conceição MM, Fernandes VJJ, Araújo AS, Farias MF, Santos IMG, Souza AG. Thermal and oxidative degradation of castor oil biodiesel. Energ Fuel. 2007;21(3):1522–7.
47. Zhang L, Zhang M, Zhou Y, Hu L. The study of mechanical behavior and flame retardancy of castor oil phosphate-based rigid polyurethane foam composites containing expanded graphite and triethyl phosphate. Polym Degrad Stabil. 2013;98:2784–94.
48. Pawlik H, Prociak A. Influence of palm oil-based polyol on the properties of flexible polyurethane foams. J Polym Environ. 2012;20:438–45.
49. Gerakines PA, Schutte WA, Greenberg JM, van Dishoeck EF. The infrared band strengths of H_2O, CO and CO_2 in laboratory simulations of astrophysical ice mixtures. Astron Astrophys. 1995;296:810–97.